Nanoscale

ARTICLE

Received 00th January 20xx,
Accepted 00th January 20xx

DOI: 10.1039/x0xx00000x

www.rsc.org/

Spatially-resolved profiling of carbon nanotube uptake across cell lines

H. D. Summers,[a] P. Rees,[a] J. T-W. Wang,[b] K. T. Al-Jamal[b]

The internalisation and intra-cellular distribution of carbon nanotubes (CNT) has been quanitatively assessed using imaging flow cytometry. Spatial analysis of the bright field images indicates the presence of a small sub-population (5% of cells) in which the internalised CNTs are packed into pronounced clusters, visible as dark spots due to strong optical scattering by the nanotubes. The area of these spots can be used as a label-free metric of CNT dose and we assess the relative uptake of charge-neutral CNTs, over a 24 hour exposure period across four cell types: J774 mouse macrophage cells, A549 and Calu-6 human lung cancer cells, MCF-7 human breast cells. The relative dose as indicated by the spot-area metric, closely correlates to results using the same CNT preparation, conjugated to a FITC-label and shows pronounced uptake by the J774 cells leading to a mean dose that is > 60% higher than for the other cell types. Spatial evaluation of dosing clusters is also used to quantify differences in uptake by J774 cells of CNTs with different surface functionalisation. While the percentage of CNT-cluster positive cells increases from 5% to 19% when switching from charge-neutral CNTs to poly-cationic, dendron functionalised CNTs, the single cell level analysis of internalised clusters indicates a lower dose per cell of poly-cationic CNTs relative to the charge-neutral CNTs. We concluded that there is dose homeostasis i.e., the population-averaged cellular dose of CNTs remained unchanged.

[a] *Centre for Nanohealth, College of Engineering, Swansea University, SA2 8PP, U.K.*
[b] *Institute of Pharmaceutical Science, Faculty of Life Sciences & Medicine, King's College London, Franklin-Wilkins Building, London SE1 9NH, United Kingdom.*
Electronic Supplementary Information (ESI) available: [details of any supplementary information available should be included here]. See DOI: 10.1039/x0xx00000x

Introduction

Research into the use of carbon nanotubes (CNTs) as drug/gene delivery vehicles is a rapidly increasing area of activity in the biomedicine field[1,2]. Because of their readily available surface and hollow interior, CNTs can carry high therapeutic payloads when altered by various chemical modifications[3–5]. An additional advantage is that their cellular internalisation can follow diverse pathways[6,7]. Both active endocytosis and passive diffusion (needle-like cell membrane penetration) have been described. To understand the cellular trafficking routes, distribution patterns and the biological fates of CNTs, there have been studies employing methods for intra-cellular detection and further quantification of CNTs. Labelling CNTs with either fluorophores or radio-isotopes are the most commonly used strategies for visualisation and/or quantification[8,9]. These methods provide superb resolution or sensitivity, respectively, but the measurements rely on the signals from the probes and the stability of these tags when used with CNTs should be taken into consideration. Raman spectroscopy and multi-photon luminescence microscopy have been developed to image CNTs utilising their intrinsic optical properties rather than by indirect detection[10–12]. Transmission electron microscopy is also a useful tool to characterise the tubular structure of CNTs with very high spatial resolution, but the involvement of laborious procedures and the requirement of trained personnel make these unfavourable routine techniques.

The most commonly used approach to cellular analysis of large numbers of cells, sufficient to provide statistical certainty, is flow cytometry. In this regard, label-free flow cytometry-based analyses provide an approach to assess the cellular interaction, internalisation and localisation of CNTs in a high-throughput fashion and label-free manner[13–18]. In this paper we present data using a recent advance in this technology – imaging cytometry. This provides images of cells analysed within a flow system and so adds the ability to discern spatial patterns of reporting agents or natural label-free reporters. Previous work in the area by Marangon et. al. demonstrated that the imaging cytometer is capable of high throughput imaging at sufficient spatial resolution to allow analysis of the intracellular translocation of CNTs[19]. In this case the optical absorption and scattering properties of the CNTs were found to be sufficiently pronounced to provide label-free analysis, based on bright-field or dark-field imaging. Other researchers have reported on the use of imaging cytometry for analysis of fluorescent[20] and metallic[21] nanoparticles, based on optical emission or scattering properties.

In this paper, we follow a similar experimental approach and analyse CNT-cell interactions from image-based metrics, acquired from all individual cells within large sample populations, using an imaging flow cytometer. We present a quantitative assessment of the relative dose and its spatial distribution within the cell and make direct comparisons of the nanoparticle pharmacology for multiple cell types and differing particle chemistry. We also concentrate on the development of label-free quantification. Comparative assessment of the uptake of differing nanoparticle types into multiple cell lines is extremely challenging when using fluorescence or light scatter, quantified at the whole cell level, as a reporting metric. This is the most commonly used approach for flow cytometry[22,23] but it requires accurate calibration of the nanoparticle optical signal from different samples, especially when the particle physio-chemical characteristics are being varied. The added discriminative power stemming from spatial resolution, offered by our method here, allows dose quantification based on area rather than intensity metrics[24,25], making the measurement robust in response to fluctuation in the reporting signal level. It also allows us to profile the internalisation dynamics of the CNTs. This provides information on the relative importance of the biological mechanisms that drive nanoparticle internalisation and the intra-cellular form of the resultant particle dose.

Experimental

Materials

Human lung cancer cells A549 (ATCC® CCL-185™), human lung cancer cells Calu-6 (ATCC® HTB-56™), human breast cells MCF-7 (ATCC® HTB-22™), and mouse macrophage cells J774 (ATCC® TIB-67™) are purchased from ATCC (USA). Minimum Essential Medium, Dulbecco's Modified Eagle Medium (DMEM), Advanced RPMI-1640 medium, penicillin/streptomycin, trypsin/EDTA, and phosphate buffered saline (PBS) were obtained from Gibco (Thermo Fisher Scientific Inc., UK). Fetal bovine serum (FBS) was purchased from First Link Ltd. (UK). BD CellFIXTM (10x concentrated) was purchased from BD Biosciences (UK).

Methods of cell culture and treatments

Synthesis of CNTs: The synthesis of poly-cationic dendron functionalised CNT (CNT(++)) has been reported previously[4,26]. The amine-functionalised CNT-FITC conjugate (CNT(+)) and its derivative with further IgG conjugation CNT(n), were synthesised following the protocols that have also been reported previously[26].

Cell culture: A549 cells were cultured in DMEM, MCF-7 cells were cultured in MEM, and Calu-6 and J774 cells were cultured in Advanced RPMI-1640 medium, all at 37°C in 5% CO_2. Culture media was supplemented with 10% FBS, 100 U/ml penicillin, 100 µg/ml streptomycin and 1% L-glutamine (Sigma). Cells were routinely grown in 75 cm^2 tissue culture flasks and passaged twice a week, after detachment with Trypsin/EDTA, when reaching 80% confluency.

For uptake studies, cells were seeded in 24-well plates (triplicates) and incubated with CNT(n), CNT(+) or CNT(++) at a concentration of 10 µg/ml for 24 h. Cells were then washed with PBS, trypsinised and collected in culture media. Collected cells were washed three times with PBS by centrifugation (200 g, 5

min) and fixed using diluted BD CellFIX (1:10) at room temperature for 15 min. Cells were centrifuged again and re-suspended in PBS. Cells were kept at 4 °C in the dark until flow cytometric analysis. Previous work[4] using two different cytotoxic assays confirmed that the dendron-functionalised CNTs were nontoxic to cells following 24 hours of exposure, up to concentrations of 80 μg/ml.

Flow cytometry

Cell images were acquired with an Imagestream 100 flow cytometer (Merck Millipore, Seattle, WA); bright field, dark field and fluorescence images were collected for each cell within sample sets of at least 10,000 cells. A 488 nm wavelength excitation laser, at a power of 100 mW was used for excitation of the FITC fluorophore. Untreated cells were imaged as controls. All image analysis was done within the Ideas software environment (Merck Millipore, Seattle, WA).

Results and discussion

CNT uptake at the population level

The quantification of content of a neutrally-charged CNT type (CNT(n))[27], based on image analysis in three channels: bright field (BF, optical transmission), dark field (DF, optical scatter at 90^0) and fluorescence was performed. Examples of the three image sets for six typical, J774 cells are shown in Figure 1.

The high optical scattering coefficient of the CNTs leads to clearly visible, dark spots in the bright field images and corresponding bright pixels in the dark field channel. The FITC signal appears as a diffuse patterning across the whole cell with additional high intensity areas, correlating to the CNT clusters, seen in the bright and dark field images. This is in agreement with our previous studies which showed that CNTs can enter cells through different pathways, with observation of individual nanotubes or CNT clusters in vesicular compartments inside cells[6,29]. The FITC signal is present in the majority of cells (96% of population), confirming that regardless of whether in diffuse or clustered form the internalisation of the nanotubes is widespread.

To assess the validity of quantifying CNT uptake using a label-free method, we compare the mean intensity per cell in the DF, FITC and BF channels for the 4 cell types. The results for a 24 hour exposure to CNT(n), are shown in Figure 2. They are based on the use of population averaged parameters and so report on the mean CNT load within each cell culture. The mean value of pixel intensity is used for the DF and FITC channels; to parameterise the BF image we use an area metric. The marked image contrast produced in the bright field channel by the CNT clusters allows masking of the dark spots using a simple thresholding of an inverted image. From this a *dark spot area* metric is obtained (Figure 2, grey bars). This is a more robust measure than the mean channel signal per cell as it is independent of signal intensity (as long as intensity is above the mask threshold).

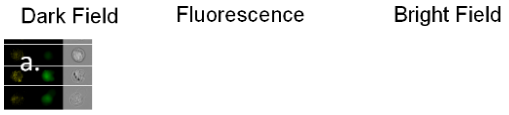

Figure 1: a.-f. Panel of typical images from the Imagestream Cytometer for J774 cells. Each cell is simultaneously imaged in a dark field, a fluorescent and a bright field channel. Incubation conditions: (CNT(n)), 24 h, 10 μg/ml.

In Figure 2a, a comparison is made of the signal intensity from CNT exposed cells (coloured bars) to that from a CNT-free control sample (black line). The signal from exposed cells is statistically different to the control in all data sets bar one (95% confidence level, all except DF signal in Calu6 cells). So the presence of the nanoparticles is reported by all three signal modalities. However, they are not all robust enough to quantify and compare the nanoparticle dose between cell types. The level of the reporting signal subtracted from the background (signal-background) is shown in Figure 2b. The results from the FITC labelled cells show that the CNT loading is greatest in the J774 cell line which is unsurprising given the phagocytic nature of this cell type. The uptake into A549 cells is ~ 40% lower whilst the MCF7 and Calu6 cells show no significant difference with both cell types having ~ 30% of the J774 CNT content. In the DF channel the high background scatter produced by the cells leads to a low signal to background ratio, especially for the MCF7 and Calu6 cells in which the control sample scatter is of an equivalent level to that produced by the CNTs (Figure 2a, black lines). Thus the DF channel cannot provide a meaningful,

statistically robust metric. The dark spot area metric from the BF channel does correlate reasonably well to the FITC signal (a quantitative label), indicating the same relative scaling of CNT levels between cell types. However, this data is also subject to large uncertainty bounds for the Calu6 cell line, where the increase in signal from the CNTs is smaller than the background value obtained from control samples.

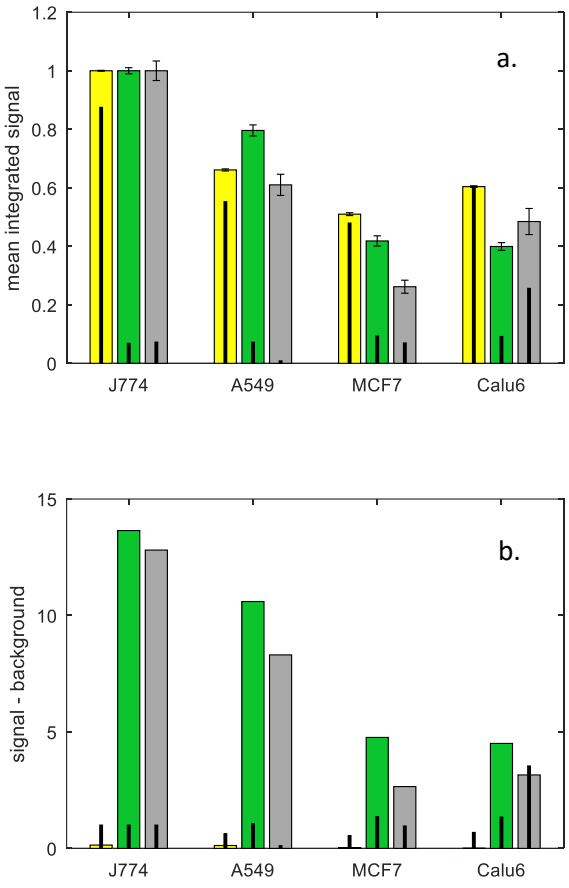

Figure 2: a. Relative signal from mean DF intensity per cell (yellow bars), mean fluorescence per cell (green bars) and area of dark spots in the BF image (grey bars). All measures are normalised to the J774 cell line value. The black lines indicate the relative size of the background signal (obtained from CNT-free cells). The error bars represent the s.e.m. (N > 2000 for all data). b. signal-background measure (background taken to be the value from control, CNT-free cell samples), normalised to the signal from the control sample for the J774 cell line. The black lines indicate the size of the background signal. Incubation conditions: (CNT(n)), 24 h, 10 µg/ml.

The image masking of dark spots allows quantification of the spatial location of CNTs as the proportion of the FITC signal within these 'dark-spot' areas can be compared to that from the whole cell. Whilst there is a higher signal density corresponding to the CNT clusters this does not constitute a large fraction of the total: In the J774 cell line the dark CNT clusters account for 4% of cell area and contain 7% of the total FITC signal. The majority of the CNT dose is therefore in a diffuse form.

CNT uptake at the single cell level

Having established that population-averaged metrics do indicate the presence of CNTs within cells, we proceed to analyse the cell-to-cell variation of these image derived parameters. We begin with a study of the correlation between DF and BF derived parameters in cells exposed to CNT(n) for 24 hours. These metrics have been used previously by Marangon *et. al.* to quantify CNT uptake in endothelial cells[19]. Scatter plots of DF intensity versus integrated BF intensity (mean per cell), for the four cell types are shown in Figure 3. The results indicate the presence of two distinct sub-populations: A majority group sits at the right hand side of the plots, close to the control population mean (black crosses in Figure 3). This group has a relatively high BF intensity and shows minimal correlation between BF and DF parameter values ($r < 0.05$). A minority group sits to the left of the plot, differentiated by a low BF channel intensity ($\log_{10}$ BF intensity < 0) and a clear anti-correlation between the BF and DF intensity values (r-range of -0.45 to -0.67). Inspection of the cell images for this minority sub-group, which constitutes ~ 5% of the total cell population, indicates the presence of pronounced dark spots in the BF image, corresponding to dense intra-cellular clusters of CNTs (see Electronic Supplementary Information, S1). These CNT clusters reduce the BF mean intensity to a value less than the image background and boost the DF signal due to their high optical scattering coefficient. We therefore label this group of cells as *'CNT-cluster positive'* (encompassed by dashed red circle in Figure 3). It should be noted that this is a classification of the sub-population which has internally agglomerated CNTs rather than that which has CNTs *per se*. The majority population on the right hand side of the plots in Figure 3 may have internalised CNTs in a diffuse form that does not significantly alter the optical transmission or scattering characteristics of these cells.

Our results for the CNT-cluster positive cells are similar to previous reports by Marangon *et. al.* using imaging cytometry[19], which also demonstrated a clear anti-correlation between dark and bright field signals ($r = -0.68$). However, in these experiments > 80% of the cells were identified as being CNT positive, whereas in our work this number is only 5%. We attribute this variance to the different cell lines and CNT type used. Similar results to those reported by Marangon *et. al.* were obtained from an extended exposure over 72 hours using a poly-cationic dendron-functionalised CNTs[4] (CNT(++)) (see Electronic Supplementary Information, S2).

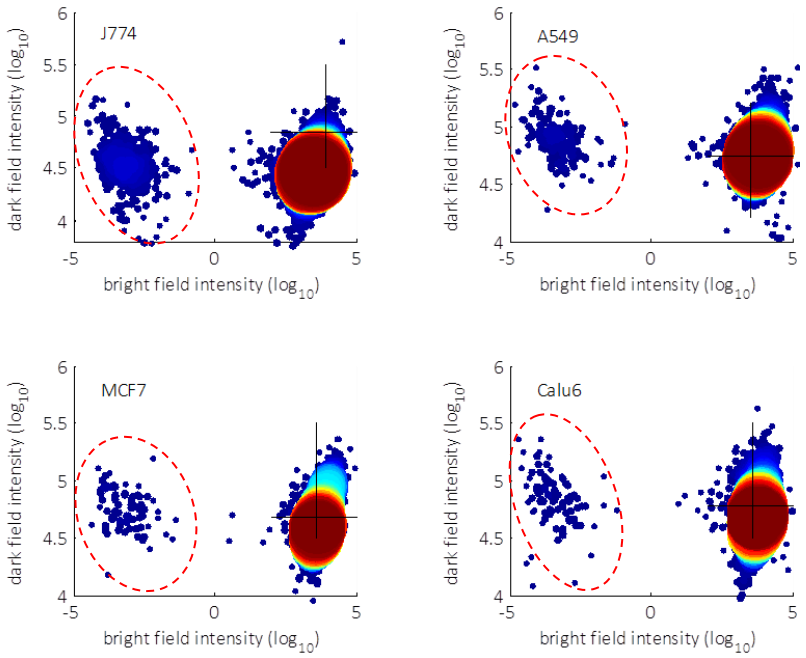

Figure 3: Scatter plots of dark field versus bright field intensity for the four cell lines (N > 2,000 in all cases). The black crosses indicate the positions of the mean values for the control samples not exposed to CNTs. The CNT-cluster positive cells (log_{10} BF < 0) are indicated by the red dashed circle. Incubation conditions: (CNT(n)), 24 h, 10 µg/ml.

Having identified the CNT-cluster positive sub-fraction of cells we can more accurately assess the relative loading profile of the four cell lines. The identification of a relatively small fraction of CNT cluster positive cells means that access to spatial information within the cell images is essential for accurate assessment of the CNT content. Whilst the population mean of the signal intensities (Figure 2) shows clear differences between cell types, this will not be representative of the true CNT content when only a small fraction of the cells contributes to the population mean. For example, the mean dark spot area reported in Figure 2 stems from a signal in ~ 100 cells averaged over all 2000+ cells.

The mean FITC fluorescence and BF dark spot area for the CNT-cluster positive group, is shown in Figure 4 (signal - background). The use of only CNT-cluster positive cells for analysis now provides a BF channel, *dark spot area* metric that is significantly greater than the control samples, for all cell types. Thus this, label-free metric can be used as a robust and quantitative indicator of the relative CNT content across the cell lines.

Determination of CNT(n) aggregate size in cells

The differences in CNT uptake shown in Figure 4 are an average over the CNT-cluster positive sub-group of cells. To profile the contribution of individual cells to this mean difference we calculate the cumulative distribution function (CDF) for the BF dark spot area metric: % of cells with a given sum total of dark areas in BF image. This is presented in Figure 5 and provides a profile of the spatial localisation of CNTs within the cell. The insert images are positioned on the x-axis to show typical cells for the particular spot area range. The data and images show that the increased loading into J774 cells (and to a lesser extent into A549 cells) is associated with larger intra-cellular clusters rather than increased numbers of clusters per cell.

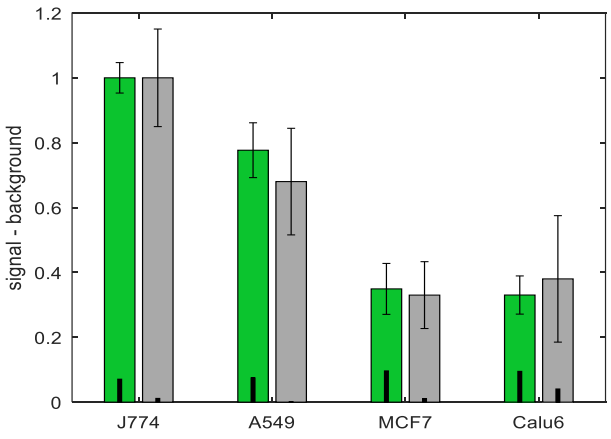

Figure 4: CNT-cluster positive, population: values for mean fluorescence per cell (green bars) and BF dark spot area (grey bars). Data represents signal – background relative to the J774 cell value. The black lines indicate the size of the background signal (from control samples). Errors bars show s.e.m. (N>140)

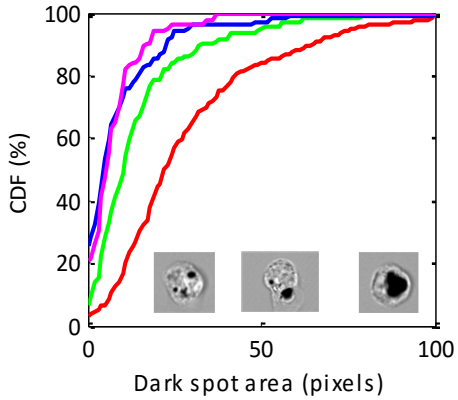

Figure 5: Cumulative distribution frequency (% of cells) of dark spot area for J774 (red line), A549 (green line), MCF7 (blue line) and Calu6 (magenta line) cells. The image inserts display cells (J774) typical for the particular range of dark spot area.

To further investigate why the J774 cell line shows a different behaviour to the other cell lines we referred to the nanotube colloidal dispersion profiles (see Electronic Supplementary Information, Table S1). The DLS measurements report indicated agglomeration of CNT(n) suspensions with poor size quality report indicating the polydisperse nature of the sample (data not shown). The presence of elevated numbers of large intra-cellular CNT clusters in the J774 cells is thus explained by the increased capacity of these phagocytic cells to internalise the CNT(n) agglomerates.

Profiling the effect of CNT surface properties

Using the J774 cell line we compared cellular CNT content following 24 hours exposure to the charge neutral (CNT(n)), amine functionalised[27] (CNT(+)) and poly-cationic dendron-functionalised CNTs[4] (CNT(++)). The results are shown in Figure 6 in the form of scatter plots of DF intensity versus BF intensity. Again, there are 2 distinct populations within each plot with a small, low BF intensity, CNT-positive group identified as having pronounced intra-cellular CNT clusters (left hand side of plots). The percentage of CNT-cluster positive cells increased with CNT surface charge: CNT(n) : 5%, CNT(+) : 9%, CNT(++): 19% (Figure 6: number of cells in left hand sub-group as a % of all cells displayed).

Thus exposure to poly-cationic CNTs produced the highest % population as previously reported using conventional side scatter analysis by flow cytometry[4]. The population of cells showing clustered internalisation of the CNT(n) is significantly smaller (Figure 6a cf. Figure 6b and 6c). Reduced aggregation of CNT (++) and CNT(+), driven by increased electrostatic repulsion among nanotubes, has been confirmed with transmission electron microscopy in our previous study[4] (see Electronic Supplementary Information, S3). Thus this reduced uptake of the CNT(n) is possibly due to their aggregation or their less pronounced surface positive charge compared to CNT (+)/(++).

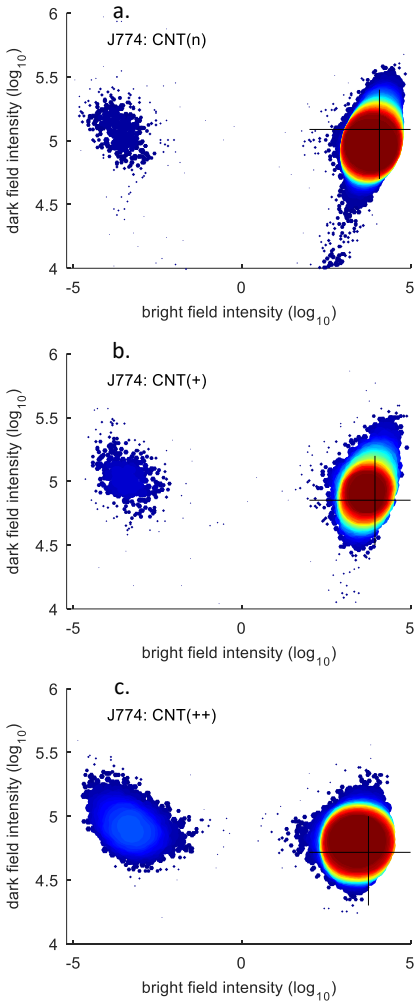

Figure 6: Scatter plots of dark field versus bright field intensity for the three CNT preparations (N > 2,000 in all cases). The black crosses indicate the positions of the mean values for the control samples not exposed to CNTs. Incubation conditions: (CNT(n)), 24 h, 10 µg/ml.

Packing density of CNT of different surface properties in J774 cells

To further investigate the form of the intra-cellular CNT clustering we analysed the relationship between total BF intensity per cell and total dark spot area in each BF J774 cell image, for the CNT-cluster positive cell population (see Figure 7), for CNT(n), CNT(+) and CNT(++). The three data sets in Figure 7 all conform to the same functional form, confirming that the relationship between mean image brightness per cell and the area of CNT-related dark spots remains the same, regardless of the CNT surface properties. This indicates that the 'packing density' of the intra-cellular clusters, which give rise to the dark

spots, is the same for all CNT types (fixed relationship between CNT cluster area and optical attenuation). Whilst the functional form of the uptake is unchanging for the different derivatives, the distribution of cells across this profile is not. In particular, there is a marked increase in number of cells with a high dark spot area when loaded with the neutral CNT(n) (Figure 7). As seen in the data from multiple cell lines (Figure 4), the agglomeration of the CNT(n) leads to pronounced clusters within the cells which are detected via the BF image analysis.

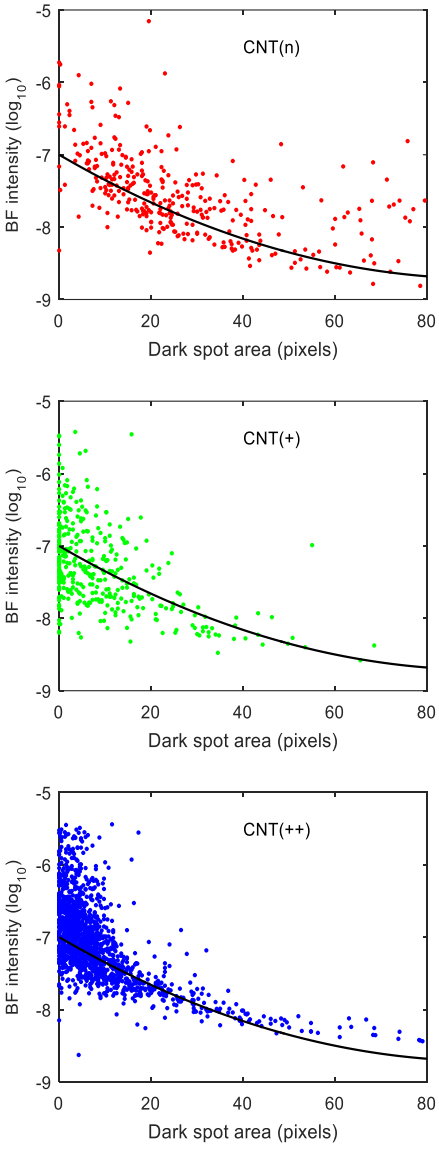

Figure 7: Scatter plots of mean bright field intensity versus dark spot area (in BF images), per cell, for J774, CNT-cluster positive cells exposed to CNT(n), CNT(+), CNT(++). The same solid black line is displayed in all plots to indicate a common trend line.

The absolute change in mean BF intensity per cell relative to the control, for the populations with clustered (CNT-cluster positive) and diffuse CNTs (CNT-cluster negative) is shown in Figure 8. There is a statistically meaningful signal reduction in all cases, thus it would appear that the presence of diffuse CNTs within the cytoplasm is sufficient to produce a measurable change in optical transmission. This data underlines the importance of spatial discrimination of the internalised CNT dose as the diffuse and clustered uptake group exhibit different trends. The agglomeration of the CNT(n) preparation produces a pronounced decrease in BF signal in those cells exhibiting clustered uptake, whilst the signal in the cell population with diffuse uptake is relatively insensitive to the type of CNT. The total CNT uptake across the cell population is a function of the dose per cell and the number of cells. For the CNT(n) preparation, the high CNT content in the population group showing internal clusters (~ 2x CNT(++) value) is offset by the low numbers of these cells (5% cf. 19%) and so the average CNT dose for the whole population is similar for all CNT types (indicated by grey bars in Figure 8).

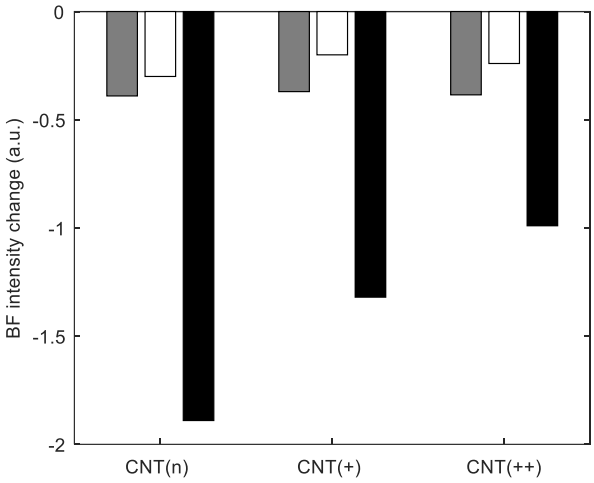

Figure 8: change in mean BF intensity per cell relative to a control sample with no CNT exposure; CNT-cluster positive sub-population (black bars), CNT-diffuse sub-population (white bars), all cells (grey bars).

Summary and conclusions

Our results show that quantification and spatial resolution of the light signal, transmitted through nanoparticle loaded cells allows label free analysis of particle dose. The validity of bright field metrics such as mean intensity per cell or area of dark spots as quantifiers of CNT dose is verified by comparison to fluorescently labelled control particles. Profiling of the CNT dose across a panel of four cell lines shows elevated uptake for phagocytic J774 cells and highly-endocytic A549 epithelial cells in comparison to Calu6 and MCF7 cell lines.

The processes of nanoparticle exposure and cell uptake are determined by the coupled interactions between particles, environment and cells[30], with complex dynamics driven by feedback loops[31] and time dependent processes[32,33]. The

resulting quantity and form of the internalised particle dose is highly dependent upon cell type and particle surface characteristics and can vary greatly from cell to cell. Nanoparticle uptake is thus poorly described by mean metrics of whole cell quantities, averaged across a population[34]. In the specific case of CNTs, their surface charge state influences the propensity to agglomerate, which then determines the relative weights of endocytic internalisation, producing internal CNT clustering, and direct trans-membrane transport leading to a diffuse cytoplasmic CNT dose. A complete understanding of this nanoparticle dosing (endocytic vs cytosolic), which can be even more crucial for nucleic acid delivery, can only be obtained through spatially resolved analyses.

Through the use of imaging cytometry we show that the spatial distribution of CNTs within cells is driven by particle-cell interactions in which particle decoration and cell type play a role. As the level of cationic charge on the CNT surface increases, it enhances adhesion to the cell membrane and reduces the amount of particle agglomeration. The changes in particle dispersion influence the relative uptake in different cell types with phagocytic cells able to internalise agglomerates of a wide size range. The spatial information obtained from imaging cytometry provides an understanding of the complex dynamics of particle uptake, which at the whole cell level are potentially misleading. Standard assessment, using whole cell metrics, indicates only small differences in mean dose per cell for CNTs of different surface charge and so points to comparable partico-kinetics. However, with further information from imaging, a very different picture emerges; a dynamic environment in which dose homeostasis results from the balance of countervailing effects: uptake of high density CNT agglomerates by few cells when using low surface charge particles or uptake of reduced numbers of disperse CNTs by an increasing number of cells as surface charge is increased.

The understanding of the dose-response relationship is an essential part of nanotherapeutic or nanotoxicological studies. The biological response to an agent can be determined in a straightforward manner by monitoring binary outcomes, e.g. occurrence of cell death or expression of a transfected gene. The assessment of nano-agent dose is much more complex and hence difficult to quantify. The accurate determination of delivered dose on a cell by cell basis is challenging and most studies report instead on population mean metrics or just quote exposure concentrations. By adopting an image-based analysis we can quantify CNT dose per cell using morphological rather than intensity-based metrics. This is a major advance as it allows for direct comparison of diverse cell types, because cell or experiment related variance due to fluorescence labelling or yield efficiency are removed. Thus the current single-agent/single cell type assay, limited in scope and application, can evolve into sophisticated in-vitro studies using multiple cell types to mimic the complexity of tissue micro-environments[35]. An additional benefit of using an imaging approach to assess dose is that it can provide information relating to biological mechanism. The packing density and spatial distribution of the intra-cellular dose can be assessed. This provides quantification of the local concentration of drug cargos inside cells (e.g. agglomerates or single CNT), which then gives indication of pathways of uptake (e.g. endocytosis or passive diffusion) – particularly relevant information when using CNTs[8]. Many nanoparticle based therapeutics target the nucleus to effect genetic reprogramming such as gene silencing[4], the dose assessment protocols presented here provide spatial discrimination of the intra-cellular dose and so could provide information on the correlation of nuclear localisation of an agent to its therapeutic effect.

Acknowledgements

Funding from BBSRC (BB/J008656/1) and Worldwide Cancer Research (12−1054) is acknowledged. The Authors also acknowledge Prof. M.-A. Herrero for providing the CNT(++) sample.

References

1 A. Bianco, K. Kostarelos and M. Prato, *Curr. Opin. Chem. Biol.*, 2005, 9, 674–679.

2 Z. Liu, S. Tabakman, K. Welsher and H. Dai, *Nano Res.*, 2009, **2**, 85–120.

3 Z. Liu, S. M. Tabakman, Z. Chen and H. Dai, *Nat. Protoc.*, 2009, **4**, 1372–82.

4 K. T. Al-Jamal, F. M. Toma, A. Yilmazer, H. Ali-Boucetta, A. Nunes, M.-A. Herrero, B. Tian, A. Eddaoudi, W. T. Al-Jamal, A. Bianco, M. Prato and K. Kostarelos, *FASEB J.*, 2010, **24**, 4354–4365.

5 S. Vardharajula, S. Z. Ali, P. M. Tiwari, E. Eroğlu, K. Vig, V. A. Dennis and S. R. Singh, *Int. J. Nanomedicine*, 2012, 7, 5361–5374.

6 L. Lacerda, J. Russier, G. Pastorin, M. A. Herrero, E. Venturelli, H. Dumortier, K. T. Al-Jamal, M. Prato, K. Kostarelos and A. Bianco, *Biomaterials*, 2012, **33**, 3334–3343.

7 K. T. Al-Jamal, H. Nerl, K. H. Müller, H. Ali-Boucetta, S. Li, P. D. Haynes, J. R. Jinschek, M. Prato, A. Bianco, K. Kostarelos and A. E. Porter, *Nanoscale*, 2011, **3**, 2627–2635.

8 N. W. S. Kam, Z. Liu and H. Dai, *Angew. Chemie - Int. Ed.*, 2006, **45**, 577–581.

9 Z. Liu, S. M. Tabakman, Z. Chen and H. Dai, *Nat. Protoc.*, 2009, **4**, 1372–82.

10 J. W. Kang, F. T. Nguyen, N. Lue, R. R. Dasari and D. A. Heller, *Nano Lett.*, 2012, **12**, 6170–6174.

11 N. Rubio, L. M. Hirvonen, E. Z. Chong, J. T. W. Wang, M. Bourgognon, H. Kafa, H. A. F. M. Hassan, W. T. Al-Jamal, D. McCarthy, C. Hogstrand, F. Festy and K. T. Al-Jamal, *Chem. Commun.*, 2015.

12 V. Neves, E. Heister, S. Costa, C. Tilmaciu, E. Borowiak-Palen, C. E. Giusca, E. Flahaut, B. Soula, H. M. Coley, J.

McFadden and S. R. P. Silva, *Adv. Funct. Mater.*, 2010, **20**, 3272–3279.
13 K. T. Al-Jamal and K. Kostarelos, in *Carbon Nanotubes: Methods and Protocols, Methods in Molecular Biology*, 2010, vol. 625, pp. 123–134.
14 D. Cai, D. Blair, F. J. Dufort, M. R. Gumina, Z. Huang, G. Hong, D. Wagner, D. Canahan, K. Kempa, Z. F. Ren and T. C. Chiles, *Nanotechnology*, 2008, **19**, 1–10.
15 I. Marangon, N. Boggetto, C. Ménard-Moyon, N. Luciani, C. Wilhelm, A. Bianco and F. Gazeau, *J. Vis. Exp.*, 2013, 1–11.
16 N. W. S. Kam, T. C. Jessop, P. A. Wender and H. Dai, *J. Am. Chem. Soc.*, 2004, **126**, 6850–6851.
17 X. Zhang, W. Hu, J. Li, L. Tao and Y. Wei, *Toxicol. Res. (Camb).*, 2012, **1**, 62–68.
18 M. H. Lamm and P. C. Ke, eds. K. Balasubramanian and M. Burghard, Humana Press, Totowa, NJ, 2010, pp. 135–151.
19 I. Marangon, N. Boggetto, C. Ménard-Moyon, E. Venturelli, M. L. Béoutis, C. Péchoux, N. Luciani, C. Wilhelm, A. Bianco and F. Gazeau, *Nano Lett.*, 2012, **12**, 4830–4837.
20 S. Vranic, N. Boggetto, V. Contremoulins, S. Mornet, N. Reinhardt, F. Marano, A. Baeza-Squiban and S. Boland, *Part. Fibre Toxicol.*, 2013, **10**, 2.
21 A. Ivask, M. Visnapuu, P. Vallotton, E. R. Marzouk, E. Lombi and N. H. Voelcker, *NanoImpact*, 2016, **1**, 29–38.
22 Y. Ibuki and T. Toyooka, *Methods Mol. Biol.*, 2012, **926**, 157–166.
23 R. M. Zucker, E. J. Massaro, K. M. Sanders, L. L. Degn and W. K. Boyes, *Cytometry. A*, 2010, **77**, 677–685.
24 H. D. Summers, P. Rees, M. D. Holton, M. R. Brown, S. C. Chappell, P. J. Smith and R. J. Errington, *Nat. Nanotechnol.*, 2011, **6**, 170–174.
25 H. D. Summers, M. R. Brown, M. D. Holton, J. A. Tonkin, N. Hondow, A. P. Brown, R. Brydson and P. Rees, *ACS Nano*, 2013, **7**, 6129–6137.
26 M. A. Herrero, F. M. Toma, K. T. Al-Jamal, K. Kostarelos, A. Bianco, T. Da Ros, F. Bano, L. Casalis, G. Scoles and M. Prato, *J. Am. Chem. Soc.*, 2009, **131**, 9843–9848.
27 J. T. W. Wang, C. Fabbro, E. Venturelli, C. M??nard-Moyon, O. Chaloin, T. Da Ros, L. Methven, A. Nunes, J. K. Sosabowski, S. J. Mather, M. K. Robinson, J. Amadou, M. Prato, A. Bianco, K. Kostarelos and K. T. Al-Jamal, *Biomaterials*, 2014, **35**, 9517–9528.
28 W. Wu, S. Wieckowski, G. Pastorin, M. Benincasa, C. Klumpp, J.-P. Briand, R. Gennaro, M. Prato and A. Bianco, *Angew. Chemie Int. Ed.*, 2005, **44**, 6358–6362.
29 K. T. Al-Jamal, H. Nerl, K. H. Müller, H. Ali-Boucetta, S. Li, P. D. Haynes, J. R. Jinschek, M. Prato, A. Bianco, K. Kostarelos and A. E. Porter, *Nanoscale*, 2011, **3**, 2627–2635.
30 M. Lundqvist, J. Stigler, G. Elia, I. Lynch, T. Cedervall and K. A. Dawson, *Proc. Natl. Acad. Sci. U. S. A.*, 2008, **105**, 14265–70.
31 C. D. Walkey, J. B. Olsen, H. Guo, A. Emili and W. C. W. Chan, *J. Am. Chem. Soc.*, 2012, **134**, 2139–2147.
32 S. Ahn, E. Seo, K. Kim and S. J. Lee, *Sci. Rep.*, 2013, **3**, 1997.
33 E. Casals, T. Pfaller, A. Duschl, G. J. Oostingh and V. Puntes, *ACS Nano*, 2010, **4**, 3623–3632.
34 M. J. Ware, B. Godin, N. Singh, R. Majithia, S. Shamsudeen, R. E. Serda, K. E. Meissner, P. Rees and H. D. Summers, *ACS Nano*, 2014, **8**, 6693–6700.
35 V. P. Chauhan and R. K. Jain, *Nat. Mater.*, 2013, **12**, 958–62.